arXiv:0704.2610v1 [cond-mat.mtrl-sci] 19 Apr 2007

Drift of charged defects in local fields as aging mechanism in ferroelectrics

Yuri A. Genenko*

Institute of Materials Science, Darmstadt University of Technology, Petersenstr. 23, 64287 Darmstadt, Germany

Doru C. Lupascu

Institute of Materials Science, Dresden University of Technology, Helmholtzstraße 7, 01069 Dresden, Germany

(Dated: February 1, 2008)

Abstract

Point defect migration is considered as a mechanism for aging in ferroelectrics. Numerical results are given for the coupled problems of point defect migration and electrostatic energy relaxation in a 2D domain configuration. The peak values of the clamping pressure at domain walls are in the range of 10^6 Pa, which corresponds to macroscopically observed coercive stresses in perovskite ferroelectrics. The effect is compared to mechanisms involving orientational reordering of defect dipoles in the bulk of domains. Domain clamping is significantly stronger in the drift mechanism than in the orientational picture for the same material parameters.

PACS numbers: 77.80.Dj,77.80.Fm,77.84.Dy,61.72.Ss

*Electronic address: yugenen@tgm.tu-darmstadt.de

I. INTRODUCTION

Ferroelectric materials underlie restrictions in technological applications because of several degradation phenomena. One of these phenomena is aging which is defined as the gradual change of material properties with time t under static external boundary conditions [1, 2, 3, 4, 5, 6, 7, 8]. Experimentally, the dielectric constant decreases and hysteresis loops alter their shape and amplitude in remanent polarization and coercive field. The dielectric constant decreases as the logarithm of time in an intermediate time range saturating for long times [9]. The change of material properties is caused by a decreasing domain wall mobility stabilizing in an aged domain structure [10]. In order to describe the experimentally observed shifted or deformed ferroelectric hysteresis loops after aging [11] the internal field $\mathbf{E}^i$ has been defined as a quantity describing the strength of domain stabilization [6]. Several mechanisms have been considered to partake in the stabilization process, space charge formation [3, 4], domain splitting [10], ionic drift [11, 12, 13], or the reorientation of defect dipoles [14]. Except for domain splitting, all mechanisms directly involve some reordering of point defects. Within a microstructure, three relevant locations can be identified for charge carrier rearrangement: the domain bulk, grain boundaries, or domain walls. For the bulk effect, defect dipoles reorient with respect to the direction of the spontaneous polarization under an electrical field or strain. For the grain boundary effect, charged point defects move under electrical fields originating from polarization discontinuities at the grain boundaries or the outer perimeter of the sample in order to compensate the fields. The same process can occur at charged domain walls and then becomes a domain wall effect [15, 16]. Local space charge is another electric driving force for ionic currents observed in $LiNbO_3$ type crystals [17, 18] as well as perovskites [19, 20, 21].

Elastic fields can provide a second driving force for defects inside domains but will not be treated here. For not too rigid non-charged domain walls, the localization of free charge carriers at a domain wall is a further possible effect entailing the wrinkling of the initially planar walls [22, 23, 24, 25]. Even though this is a physically interesting mechanism, it will not be taken into consideration here.

Oxygen vacancies are a well known and frequent defect in the perovskite structure. They have been considered to play an important role in aging of ferroelectric materials due to their low, but finite mobility. In the orientational picture, oxygen vacancies, when adjoint

to an acceptor center, form electric and elastic defect dipoles in the bulk of a ferroelectric domain [6]. The defect dipoles align parallel to the spontaneous polarization P_s by diffusion of the mobile oxygen vacancy in cage motion. Because of the relatively slow oxygen vacancy motion [26], the polarization directions of the aligned defect dipoles stay constant when the direction of P_s changes for short times. In this case, the defect dipoles generate an internal electrical field $\mathbf{E}^i$ which stabilizes the domain pattern by increasing the force constant for the reversible displacement of the domain walls [27]. This relaxation model has been well developed [28]. It bears two insufficiencies, though, the time dependence of aging is not reproduced and the absolute values of clamping pressures are low [29]. A second point of view about the role of oxygen vacancies in aging is the formation of ionic space charges [30] which was originally proposed to explain space charge effects in $BaTiO_3$ single crystals [31]. Ionic space charges are well known for highly doped positive temperature coefficient resistors based on $BaTiO_3$ [32]. For aging the mobile charge carriers move to charged domain faces or grain boundaries and compensate polarization. This leads to an asymmetric charge distribution whereby a voltage offset arises yielding the known shift or deformation of the ferroelectric hysteresis [33]. The clamping pressure on domain walls generated by these space charges has not been treated mathematically for periodic domain structures.

This paper describes quantitatively the formation of space charges in single domains of a periodic structure and shows the development of the defect distribution inside the domain. An estimate of bending and clamping pressures on domain walls and a comparison to the orientational picture [14] are given. Electrostatic clamping of domain walls through the formation of space charges is calculated to be two orders of magnitude stronger than clamping through aligned defect dipoles for the same concentration of charge carriers.

The model is independent of the type of point defect, as long as a diffusion constant can be assigned and the defect is charged. It can thus be equally well applied to hopping of electronic carriers. The oxygen vacancy was chosen for the numerical examples in order to be comparable to previous work, but does not preclude a statement on the physical nature of the mobile carrier.

II. GENERAL MODEL

In order to study the effect of migration of charge carriers on aging, we chose a two-dimensional periodic array of domains cut by the grain surface, $z = 0$, perpendicular to the direction of spontaneous polarization which is along the z axis in Fig. 1. This model configuration is well-known in the physics of polarized media and was used for the study of equilibrium and dynamic properties of ferromagnetic [34, 35] and ferroelectric [36, 37] materials. We assume for simplicity an isotropic material of the grain occupying the area $z > 0$ characterized by the relative dielectric constant ε_f. The dielectric material outside the grain is assumed isotropic too and is characterized by the relative permittivity ε_d. As we previously showed by finite element simulation, the electric fields arising due to spontaneous polarization in a periodic multi-domain grain of finite dimensions generate a nearly perfect periodic pattern except for the very edges of the grain [29]. We thus consider the periodic domain array of Fig. 1 occupying the semi-space $-\infty < x < \infty$, $z > 0$ as a representative model for a multi-domain grain of domain width a much smaller than the typical grain size. Due to polarization, the domain faces at $z = 0$ are alternatively charged with the

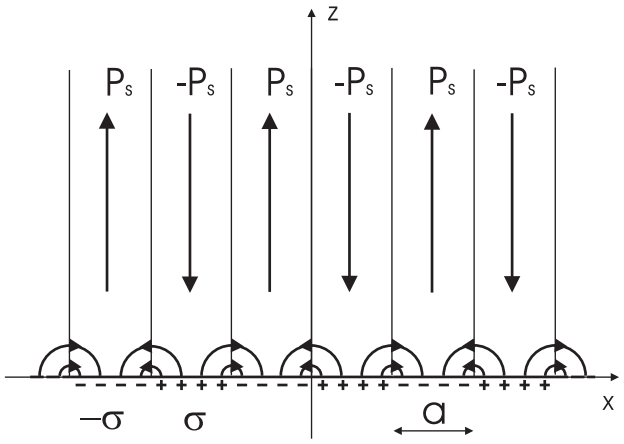

FIG. 1: Scheme of a 2D-array of 180°-domain walls crossing the grain boundary at a right angle. Straight arrows show the direction of the polarization and curved arrows the approximate directions of the local electric fields.

bound surface charge density $\sigma = |\mathbf{P}_s|$, the spontaneous polarization value. If the length of the domains L along the z-axis is much larger than their width a along the x-axis, which is typically the case in experiment, field lines are effectively closed at the same side of the grain

(see Fig. 1). As a consequence, both components of the electric field $\mathbf{E}^0(x,z)$ induced by the alternating surface charge exponentially decrease towards the interior of the grain along the z-axis [29]. Migration of the charged defects driven by the field $\mathbf{E}^0(x,z)$ is then expected to occur in a volume near the grain surface. The domains may therefore be considered infinitely long along the z-axis without introducing a substantial error.

Let us now derive the equations of evolution for the charge and field distributions in the considered system. At any time t, the electric field $\mathbf{E}(x,z,t)$ is determined by the charged faces of the domains and the imbalanced charge density of free carriers $\rho(x,z,t) = q_f\left[c(x,z,t) - c_0\right]$ through Gauss' law

$$\nabla\mathbf{E} = \frac{q_f}{\varepsilon_0\varepsilon_f}(c - c_0) \tag{1}$$

where $c(x,z,t)$ is the local concentration of mobile carriers of charge q_f, c_0 is the background concentration of the immobile charge carriers of opposite polarity warranting total electroneutrality, and ε_0 is the permittivity of vacuum. In the initial state, the system is locally neutral assuming $c(x,z,0) \equiv c_0$, the electric field $\mathbf{E}(x,z,0) \equiv \mathbf{E}^0(x,z)$ is yet to be found.

In presence of an electric field and a gradient of concentration, the flow of charge carriers is given by the sum of drift and diffusion contributions to the particle current density:

$$\mathbf{s} = \mu c\mathbf{E} - D\nabla c \tag{2}$$

where μ and D are the mobility and diffusivity of charge carriers, respectively. We assume, for simplicity, that the latter two quantities are isotropic and connected by the Einstein relation, $D = \mu k\Theta/q_f$ with k the Boltzmann constant and Θ the absolute temperature. Migration of charge carriers is governed by the continuity equation:

$$\partial_t c = -\nabla(\mu c\mathbf{E}) + D\triangle c. \tag{3}$$

For boundary conditions to the system of equations (1) and (3) we assume chemical and electrical isolation of the grain. The first requirement means vanishing particle current

$$s_z = \mu c E_z - D\partial_z c = 0, \tag{4}$$

at the grain boundary, $z = 0$. The second requirement means vanishing total electric current,

$$q_f(\mu c E_z - D\partial_z c) + \varepsilon_0\varepsilon_f\partial_t E_z = 0, \tag{5}$$

at $z = 0$ which results in a constant value of the z-component of the electric field at the grain boundary, $\partial_t E_z(x, 0, t) = 0$.

Eqs. (4,5) together with Eqs. (1,3) complete the statement of the problem of charge segregation in a ferroelectric grain. In the next section we will observe how the system relaxes according to the equations of evolution (1,3).

III. SOLUTION OF THE EQUATIONS OF EVOLUTION

In this section we first calculate the field $\mathbf{E}^0(x, z)$ in the virgin state of the system before the process of charge segregation starts. Then we formally solve equation (1) and find the total electric field $\mathbf{E}(x, z, t)$ for an arbitrary right-hand side. Finally, using the latter result, we numerically solve equation (3), self-consistently describing drift and diffusion of the mobile charge defects in the domain arrangement of Fig. 1.

A. Electric field in the virgin state of a multi-domain grain

To use the bilateral symmetry of the problem, the origin is chosen in the center of the positively charged domain face as shown in Fig. 2.

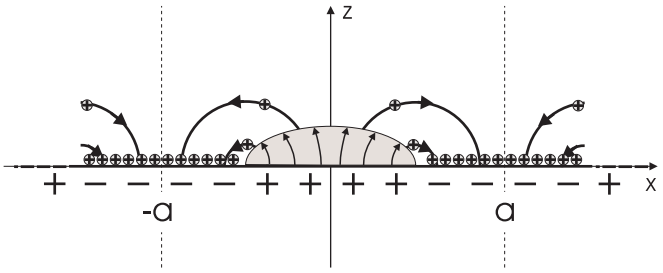

FIG. 2: Scheme of expected charge redistribution induced by the local electric field within the central region $-a < x < a$, $z > 0$, presenting repeating element of the periodic domain arrangement of Fig. 1. Thin layers of positive charge carriers piled up at the negatively charged domain faces as well as a wide (shaded) area depleted of mobile charge carriers near the positively charged domain face are shown.

The bound charge density of the domain faces is represented by an alternating function

[35]

$$\rho_b(x,z) = \sigma\delta(z)\sum_{n=-\infty}^{\infty}(-1)^n\theta\left(\frac{a}{2}-an+x\right)\theta\left(\frac{a}{2}+an-x\right), \tag{6}$$

where $\delta(z)$ and $\theta(x)$ are the Dirac δ-function and the Heaviside unit step function, respectively. The electrostatic potential induced by this bound charge is given by the expression:

$$\varphi_b(x,z) = -\frac{1}{2\pi\varepsilon_0(\varepsilon_f+\varepsilon_d)}\int_{-\infty}^{\infty}dx_0\int_{-\infty}^{\infty}dz_0\,\rho_b(x_0,z_0)\ln\left[\left(\frac{x-x_0}{a}\right)^2+\left(\frac{z-z_0}{a}\right)^2\right] \tag{7}$$

in both areas $z \geq 0$ and $z < 0$. The formula (7) is simply a superposition of the potentials generated by straight parallel charged lines located at the grain boundary $z = 0$ between the media with dielectric constants ε_d and ε_f [35].

The z-component of the electric field created by the bound charge, $\mathbf{E}^0 = -\nabla\varphi_b$, may be directly calculated by substitution of ρ_b, Eq. (6), into Eq. (7) and subsequent summation [38] which results in the form

$$E_z^0(x,z) = \frac{2\sigma}{\pi\varepsilon_0(\varepsilon_f+\varepsilon_d)}\arctan\left[\frac{\cos(\pi x/a)}{\sinh(\pi z/a)}\right] \tag{8}$$

valid for both media.

Direct calculation of the other field component, $E_x^0 = -\partial_x\varphi_b$, is more complicated because of slow convergence of the appropriate series. Instead, E_x^0 may be calculated for $z > 0$ from Gauss' law $\nabla\mathbf{E}^0 = 0$, taking into account that, from the symmetry of the problem, $E_x^0(0,z) = E_x^0(\pm a,z) = 0$. Proceeding with integration of the latter Gauss' equation over distance along the x-axis and using the mentioned boundary conditions one finds the form

$$E_x^0(x,z) = \frac{\sigma}{\pi\varepsilon_0(\varepsilon_f+\varepsilon_d)}\ln\left[\frac{\cosh(\pi z/a)+\sin(\pi x/a)}{\cosh(\pi z/a)-\sin(\pi x/a)}\right] \tag{9}$$

valid inside and outside the grain. Both field components exhibit periodic dependence along the x-axis, as expected from the periodic domain arrangement, and exponentially decrease at large distance from the charged surface $|z| \gg a$, as expected from the previous finite element simulations [29]. We note here that the short range fields, Eq. (8,9), may be very large. For example, in $BaTiO_3$ the depolarization field amplitude may be as high as $10^8\,\mathrm{V/m}$ [29]. The presence of high local fields were confirmed at least partly in observations on the acceptor doped $BaTiO_3$, where internal fields were experimentally found in the range of $10^5\,\mathrm{V/m}$ for up to 1 mol% Ni-doping and temperatures below 80°C [6].

B. Electric field due to redistribution of charged defects

At any arbitrary moment, the total electric field in the system may be conveniently decomposed as $\mathbf{E} = \mathbf{E}^0 + \mathbf{E}^i$, where the field $\mathbf{E}^0$ is determined by the charged faces of the domains, Eqs. (8,9), and the field $\mathbf{E}^i$ is generated by the distribution of the charge density in the area $z > 0$. Thanks to periodicity and the bilateral symmetry of the initial conditions, both the charge density and the electrostatic potential remain periodic and bilaterally symmetric in the course of the charge redistribution, as illustrated in Fig. 2. This allows us to consider the region $-a < x < a$ as a repetitive basic unit of the system and confine ourselves to the consideration of processes in this area. To get a full description of the electric field under these circumstances, it is sufficient to construct the Green's function of the symmetrical Neumann problem in the mentioned region, $G_s(x, z|x_0, z_0)$, so that the electrostatic potential induced by redistribution of charged defects with $z_0 > 0$ may then be presented in a form [39]

$$\varphi_i(x, z, t) = \int_0^a dx_0 \int_0^\infty dz_0\, \rho(x_0, z_0, t) G_s(x, z|x_0, z_0), \tag{10}$$

followed by the field expression $\mathbf{E}^i = -\nabla\varphi_i$.

The Green's function satisfies the equation

$$\triangle G_s(x, z|x_0, z_0) = -\frac{1}{\varepsilon_0\varepsilon_f}\delta(z - z_0)\left[\delta(x - x_0) + \delta(x + x_0)\right] \tag{11}$$

with boundary conditions $\partial_x G_s(x = \pm a, z|x_0, z_0) = 0$. The latter requirement is a consequence of the constraint $E_x(\pm a, z) = 0$ inherent to the chosen domain arrangement. Boundary conditions for the electrostatic potential, Eq. (10), on the interface between the two media at $z = 0$ [39] impose two additional boundary conditions on the Green's function

$$\begin{gathered} G_s(x, -0|x_0, z_0) = G_s(x, +0|x_0, z_0) \\ \varepsilon_d \partial_z G_s(x, -0|x_0, z_0) = \varepsilon_f \partial_z G_s(x, +0|x_0, z_0) \end{gathered} \tag{12}$$

Using the fundamental solution of the 2D Poisson equation [39] and taking into account periodicity of the problem the solution of Eq. (11) may be reduced to summation of a series:

$$G_s(x, z|x_0, z_0) = -\frac{1}{2\pi\varepsilon_0(\varepsilon_f + \varepsilon_d)} \sum_{n=-\infty}^{\infty} \left\{ \ln\left[\left(\frac{x - x_0}{a} - 2n \right)^2 + \left(\frac{z - z_0}{a} \right)^2 \right] \right\} + (x_0 \to -x_0) \tag{13}$$

for the area $z < 0$ and

$$G_s(x,z|x_0,z_0) = -\frac{1}{4\pi\varepsilon_0\varepsilon_f}\sum_{n=-\infty}^{\infty}\left\{\ln\left[\left(\frac{x-x_0}{a}-2n\right)^2+\left(\frac{z-z_0}{a}\right)^2\right]\right.$$
$$\left.+\frac{\varepsilon_f-\varepsilon_d}{\varepsilon_f+\varepsilon_d}\ln\left[\left(\frac{x-x_0}{a}-2n\right)^2+\left(\frac{z+z_0}{a}\right)^2\right]\right\}+(x_0\to -x_0) \qquad (14)$$

for the area $z > 0$.

Because of slow convergence of this series it is more convenient to perform summation for the derivatives $\partial_x G_s$ and $\partial_z G_s$ and then to restore the function G_s itself by integration using boundary conditions. This leads after all to the solution of Eq.(11)

$$G_s(x,z|x_0,z_0) = -\frac{1}{2\pi\varepsilon_0(\varepsilon_f+\varepsilon_d)}\ln\left[\cosh\frac{\pi(z-z_0)}{a}-\cos\frac{\pi(x-x_0)}{a}\right]+(x_0\to -x_0) \qquad (15)$$

for the area $z < 0$ and

$$G_s(x,z|x_0,z_0) = -\frac{1}{4\pi\varepsilon_0\varepsilon_f}\left\{\ln\left[\cosh\frac{\pi(z-z_0)}{a}-\cos\frac{\pi(x-x_0)}{a}\right]\right.$$
$$\left.+\frac{\varepsilon_f-\varepsilon_d}{\varepsilon_f+\varepsilon_d}\ln\left[\cosh\frac{\pi(z+z_0)}{a}-\cos\frac{\pi(x-x_0)}{a}\right]\right\}+(x_0\to -x_0) \qquad (16)$$

for the area $z > 0$, which are periodic, bilaterally symmetric and satisfy the proper boundary conditions. Now, from the expressions (10,15,16), the components of the electric field induced by the redistribution of charged defects may be obtained. It is easy to verify that the total electric field satisfies the boundary condition $E_x(x = \pm a, z) = 0$ for any bilaterally symmetric charge density $\rho(x, z, t)$.

C. Numerical solution of the evolution equations

Having solved equation (1) explicitly allows for the implementation of a simple direct Euler scheme for numerical treatment of the problem. Space and time will be discretized. At every time step, the change in the carrier concentration will be calculated from the previous values of the concentration and the electric fields using Eq. (3). Then, the updated values of the field will be calculated directly from the updated values of the concentration using Eq. (10). The calculation is repeated until convergence. Taking into account the bilateral symmetry of the problem, it is sufficient to consider the charge redistribution within the area $0 < x < a$.

We first introduce dimensionless variables which is helpful for the following numerical analysis and reveals those parameters of the system which are relevant to the relaxation process. Dimensionless coordinates are naturally introduced as $X = x/a$ and $Z = z/a$. The dimensionless field $\mathbf{F} = \mathbf{E}/E^*$ is expressed in units of the characteristic value $E^* = \sigma/2\varepsilon_0\varepsilon_f$. The system reveals two characteristic time scales: the drift time $\tau_\mu = a/\mu E^*$ and the diffusion time $\tau_D = a^2/D$. For the typical parameters involved, $\tau_D \gg \tau_\mu$ therefore we will introduce dimensionless time as $T = t/\tau_\mu$. The concentration of defects is now reduced to $n(X, Z, T) = c(x, z, t)/c^*$ with the characteristic value $c^* = \sigma/2aq_f$. The latter has the physical meaning of a concentration of defects on an area a^2, which completely neutralizes the bound charge σ at the domain faces. The reduced initial concentration $n_0 = c_0/c^*$ measures whether the density of defects is high or low with respect to the charge compensation concentration.

The continuity equation (3) now acquires the form

$$\partial_t n = -n(n - n_0) - \mathbf{F}\nabla n + \beta\triangle n \tag{17}$$

where all differentiations are performed with respect to the dimensionless variables. The parameter $\beta = \tau_\mu/\tau_D \ll 1$ characterizes a weak contribution of diffusion to the migration of defects in ferroelectrics. It is now seen from Eq. (17) that only two composed parameters, n_0 and β, control the relaxation process.

Though the parameter β may be rather small, it cannot be neglected as is clearly seen from the boundary condition for the particle current, Eq. (4), taken in a dimensionless form

$$nF_y - \beta\partial_y n = 0, \quad Z = 0, \tag{18}$$

otherwise this boundary condition is not compatible with the initial conditions. The finite value of β means compensation of the drift contribution to the current by the diffusion contribution at the grain boundary and this way defines the structure of a thin layer of charged defects piling up at this boundary.

Eq. (17) is supplemented by expressions for the dimensionless field $\mathbf{F} = \mathbf{F}^0 + \mathbf{F}^i$ which can be easily derived from Eqs. (8,9) and (10,15,16), namely,

$$F_x^0(X, Z) = \frac{1}{\pi}\frac{2\varepsilon_f}{\varepsilon_f + \varepsilon_d}\ln\left[\frac{\cosh\pi Z + \sin\pi X}{\cosh\pi Z - \sin\pi X}\right]$$
$$F_z^0(X, Z) = \frac{2}{\pi}\frac{2\varepsilon_f}{\varepsilon_f + \varepsilon_d}\arctan\left[\frac{\cos\pi X}{\sinh\pi Z}\right] \tag{19}$$

and

$$F^i_{x,z}(X,Z,T) = \int_0^1 dX_0 \int_0^\infty dZ_0\, f_{x,z}(X,Z|X_0,Z_0)\,[n(X_0,Z_0,T) - n_0] \tag{20}$$

where the kernels in this integral are presented by the functions

$$\begin{aligned} f_x(X,Z|X_0,Z_0) &= \frac{\varepsilon_f}{2(\varepsilon_f+\varepsilon_d)} \frac{\sin\pi(X-X_0)}{\cosh\pi(Z-Z_0)-\cos\pi(X-X_0)} + (X_0 \to -X_0), \\ f_z(X,Z|X_0,Z_0) &= \frac{\varepsilon_f}{2(\varepsilon_f+\varepsilon_d)} \frac{\sinh\pi(Z-Z_0)}{\cosh\pi(Z-Z_0)-\cos\pi(X-X_0)} + (X_0 \to -X_0) \end{aligned} \tag{21}$$

for $Z < 0$ and by functions

$$\begin{aligned} f_x(X,Z|X_0,Z_0) &= \frac{1}{4}\left[\frac{\varepsilon_f-\varepsilon_d}{\varepsilon_f+\varepsilon_d} \frac{\sin\pi(X-X_0)}{\cosh\pi(Z+Z_0)-\cos\pi(X-X_0)}\right. \\ &\quad \left. + \frac{\sin\pi(X-X_0)}{\cosh\pi(Z-Z_0)-\cos\pi(X-X_0)} + (X_0 \to -X_0)\right], \\ f_z(X,Z|X_0,Z_0) &= \frac{1}{4}\left[\frac{\varepsilon_f-\varepsilon_d}{\varepsilon_f+\varepsilon_d} \frac{\sinh\pi(Z+Z_0)}{\cosh\pi(Z+Z_0)-\cos\pi(X-X_0)}\right. \\ &\quad \left. + \frac{\sinh\pi(Z-Z_0)}{\cosh\pi(Z-Z_0)-\cos\pi(X-X_0)} + (X_0 \to -X_0)\right] \end{aligned} \tag{22}$$

for $Z > 0$.

Since the system remains electrically neutral within the domain of integration during the redistribution of defects, arbitrary constants may be added to the kernels (21,22) without changing the results of integration in Eqs. (20). This property is used in the numerical procedure to facilitate the conversion of the integrals in Eqs. (20).

As an example, we now consider the aging process in $BaTiO_3$. For the numerical simulations, the material parameters of $BaTiO_3$ at room temperature are taken from Wernicke and Jaffe et al. [40, 41], namely, $P_s = 2.71 \cdot 10^{-5}\,\mathrm{C/cm^2}$, $\varepsilon_f = 170$, $\mu = 1.73 \cdot 10^{-20}\,\mathrm{m^2/Vs}$, $a = 0.5\mu\mathrm{m}$ and q_f twice the elementary charge, implying positively charged oxygen vacancies as mobile defects. For the dielectric medium between ferroelectric grains we take the same but non-polarized material with $\varepsilon_d = 170$. This yields $c^* = 1.69 \cdot 10^{18}\,\mathrm{cm^{-3}}$, $\tau_\mu = 1.61 \cdot 10^5\,\mathrm{s}$, $\tau_D = 1.14 \cdot 10^9\,\mathrm{s}$. As was shown in one dimensional simulations [29], the parameter $\beta << 1$ has no effect on the dynamics of the relaxation. The only physical characteristic depending on $\beta << 1$ is the thickness of the positively charged layer of defects piling up at the negative face of the domain. To make this layer visible in figures and to avoid numerical problems invoked by the strong gradients of the defect density we take the value $\beta = 5 \cdot 10^{-2}$ instead of the actual ratio $\tau_\mu/\tau_D = 1.4 \cdot 10^{-4}$ for our simulations.

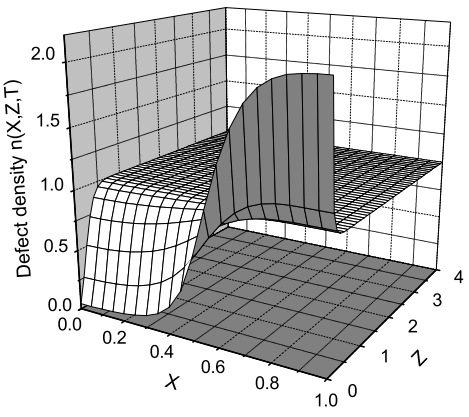

FIG. 3: Distribution of oxygen vacancies $c_{V_o}(X, Z)$ over the reference area $0 < X < 1, 0 < Z < 4$ at time $T = 0.05$ for an initial concentration of defects $c_0 = c^* = 1.69 \cdot 10^{18}$ cm^{-3}.

A snapshot of the development of the defect concentration profile over the reference area $0 < X < 1$, $0 < Z < 4$ starting with the background defect concentration $n_0 = 1$ is presented in Fig. 3 for the moment $T = 0.05$. A wide depleted zone forms near the positively charged face at $0 < X < 0.5, Z = 0$ and a very thin excess charge layer of high concentration near the negatively charged face at $0.5 < X < 1, Z = 0$.

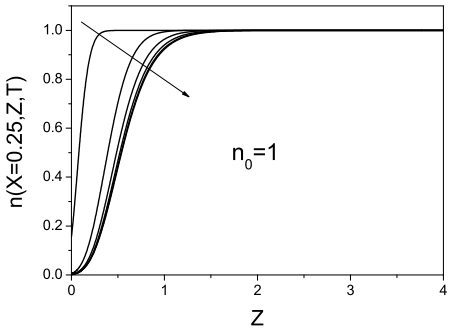

FIG. 4: Defect concentration profile along the line $X = 0.25$ for a succession of times $T =$ 0.1, 1, 2, 3, 4, 5 (from left to right) for the initial concentration of defects $c_0 = n_0 \cdot c^*$.

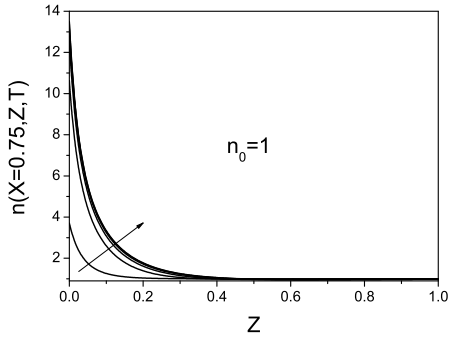

FIG. 5: Defect concentration profile along the line $X = 0.75$ for a succession of times $T = 0.1$, 1, 2, 3, 4, 5 (from left to right) for an initial concentration of defects $c_0 = n_0 \cdot c^*$.

The structural difference of these two space charge areas is better seen in Figs. 4 and 5 presenting vertical cross sections of the concentration profile along the lines $X = 0.25$ and $X = 0.75$, respectively. A succession of snapshots of the concentrations along the line $X = 0.25$ (Fig. 4) exhibits the evolution of the charge defect density near the positive face of the domain. The profile positions at the moments $T = 4$ and 5 cannot be discerned any more which indicates saturation at time $T \simeq 5$ (corresponding to $t \simeq 8 \cdot 10^5$ s). The characteristic width of this zone in the final relaxed state is of the order of unity. The defects piling up near the negative face of the domain form a much thinner layer of a characteristic width of the order of β as is represented by concentration profiles along the line $X = 0.75$ in Fig. 5. The final relaxed state is reached also at about $T \simeq 5$. The corresponding evolution of the front cross section of the concentration profile along the line $Z = 0$ shown in Fig. 6 exhibits saturation at about $T \simeq 5$, too.

In our model, drift-dominated migration of the charged defects is caused by local electric fields near the charged faces of a grain. This migration process only stops, if either no mobile defects remain in the area where fields are present or there is no remaining field in the area where the defect concentration is not zero. The process of field compensation due to defect migration is exemplified by the evolution of the electric field component $F_z = F_z^0 + F_z^i$ at the line $Z = 2$ represented in Fig. 7. F_z^i saturates at the values opposite to the local values of the initial electric field F_z^0 determined by the bound surface charge. Relaxation leads to an energy minimum where the system will resist any change of the domain wall positions.

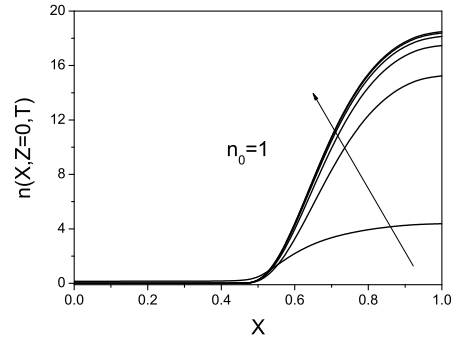

FIG. 6: Defect concentration profile along the line $Z = 0$ for a succession of times $T =$ 0.1, 1, 2, 3, 4, 5 (upwards) for the initial concentration of defects $c_0 = n_0 \cdot c^*$.

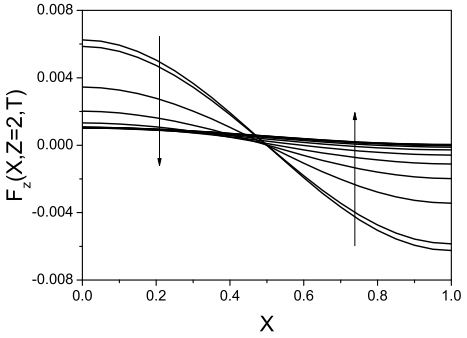

FIG. 7: The electric field component F_z plotted along the line $Z = 2$ for a succession of times $T = 0$, 0.1, 1, 2, 3, 4, 5, 6, 7, 8, 9, 10 in a system with the initial concentration of defects $c_0 = c^*$. The arrows show the direction of evolution.

The final distribution of free charges then determines the equilibrium domain configuration of the system. For an effectively low mobility of the free charge carriers the transition above the Curie point will not readily rearrange the charge carrier configuration due to thermal excitation. The defect charge density then determines the subsequent domain configuration after re-cooling the sample to low temperature. Experimentally it is observed that the original domain configuration is reproduced to a great extent [7, 8, 42].

IV. FORCES EXERTED UPON A DOMAIN WALL

From the known development of the charge density and the electric field in our model, the time dependent forces exerted upon domain walls can be evaluated. Using the general formula derived by Nechaev et al. [43] and taking into account only electrostatic contributions to the energy one can obtain the local pressure f exerted upon a wall. For a straight rigid wall considered here, one finds $f = 2\mathbf{PE}$ where $\mathbf{P}$ and $\mathbf{E}$ are the local values of spontaneous polarization and electric field, respectively. This relation is reduced, in the geometry of Fig. 1, to $f = 2P_sE_z$ (note that, in the case of the same arrangement of the 90°-domain walls, the σ would merely decrease by a factor of $\sqrt{2}$ and the force by a factor of 2, the configuration and results are otherwise identical).

Although only one end of the domains is present in the mentioned geometry of Fig. 1 it is obvious that similar segregation of the charged defects occurs on the other end of the domain, too. This results in the antisymmetric force of opposite sign exerted upon the domain wall on the other end of the domain yielding a total force equal to zero. This force cannot move the domain wall as a whole or prevent its motion but it may lead to bending of the wall violating our assumption of rigid straight domains. This is frequently encountered in real systems. Domains forming needle tips near external interfaces are commonly observed [44, 45]. In this case, part of the compensation arises within the bulk and not only right at the grain interface. The final defect distributions will be different from the case calculated here, but the essential effect of bending will remain the same. Our model of drift of free charge carriers also supports a coalescence of domains rather than their splitting. Without any further details included in the model, it contradicts the experimental observations of Ikegami ad Ueda of domain splitting during aging [10].

The evolution of the bending pressure $f(T)$ averaged over half the domain wall length, assumed as long as $L = 20a$, is shown in Fig. 8 for three different values of the initial background concentration of defects. It is seen that systems with smaller concentrations need an inversely longer time to relax. For the system with $n_0 = 1$ it takes about $T \simeq 5$ while for the system with $n_0 = 0.5$ this time is roughly doubled. All curves can be well fitted by the exponential form $f_0 \tanh(\alpha n_0 T/2)$ where the parameters $f_0 \simeq 1$ MPa and $\alpha \simeq 1$ and slowly increase when n_0 decreases. A reliable simulation of defect concentrations smaller than $n_0 = 0.5$ is impossible on the chosen template ($0 < X < 1$, $0 < Z < 4$) since in this

case migration involves defects from a wider area in order to compensate the bound charge at the domain faces.

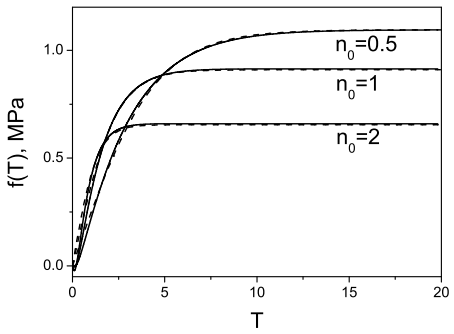

FIG. 8: Bending pressure f as a function of time $T = t/\tau_\mu$ at room temperature for $BaTiO_3$ is plotted for three different sample concentrations of oxygen vacancies $c_0 = n_0 \cdot c^*$ with $n_0 = 0.5$, 1 and 2 (solid lines). Dashed lines show fitting of the pressure by the function $f_0 \tanh(\alpha n_0 T/2)$ with parameters $f_0 = 1.095$, 0.91, 0.66 MPa and $\alpha = 0.91$, 0.86, 0.76 for $n_0 = 0.5$, 1 and 2, respectively.

One more general feature of time dependencies of the bending pressure in Fig. 8 is worth discussion. All the curves exhibit a small region at small times where the value of pressure is negative. This is not an artefact of the numerical discretization procedure but has a physical meaning. Indeed at any time, the characteristic width of the positive space charge zone near the domain face $0.5 < X < 1, Z = 0$ is of the order of β which follows from the boundary condition, Eq. (4). On the other hand, at the very beginning of charge defect migration, the characteristic width of the negative space charge zone in the area $0 < X < 0.5, Z > 0$ is less than β. This means that a negative value of the field component F_z prevails at the domain wall at this stage. This is confirmed by the dependence of F_z on position Z for different times as presented in Fig. 9.

The above considered bending force does not directly describe the aging phenomenon as long as rigid straight domain walls are retained. In fact, the total force exerted upon the walls remains equal to zero during the defect redistribution if both ends of the domains are taken into account. Nevertheless, the loss of domain wall mobility characteristic of aging may be captured in this model, too. Indeed, the segregation of charge carriers in the fixed domain framework of Fig. 1 leads to the relaxation of the energy of the electrostatic

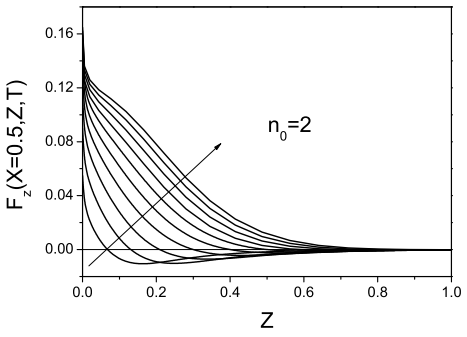

FIG. 9: Snap-shots of the distribution profile of the field component F_z along the domain wall for the succession of times $T = 0.1$, 0.2, 0.3, 0.4, 0.5, 0.6, 0.7, 0.8, 0.9, 1 (upwards) for $BaTiO_3$ at room temperature for an oxygen vacancy concentration $c_0 = n_0 \cdot c^*$.

depolarization field. The decrease of this energy per unit length of domain wall measures the clamping pressure preventing the displacement of the wall from the energy minimum:

$$P_{cl}(z,t) = \frac{\varepsilon_0 \varepsilon_f}{2a} \int_0^a dx \left(\mathbf{E}^0(x,z)^2 - \mathbf{E}(x,z,t)^2 \right) \tag{23}$$

The dependence of this pressure along the length of the wall is shown in Fig. 10 for a succession of times. The magnitude of the pressure saturates as expected at about a time $T \simeq 5$ for a defect concentration of $c_0 = c^*$. The corresponding peak value of the pressure around 1.5 MPa is comparable with the average bending pressure at the wall, Fig. 8. The magnitude of the saturated pressure increases monotonously with the defect concentration c_0 as is seen from Fig. 11.

The irreversible migration of charged defects entails growing immobilization of the domain walls and, consequently, enhancement of the coercive field, E_c. To estimate this effect one should compare the pressure $\sim P_s \mathcal{E}$ exerted by the external field, $\mathcal{E}$, upon a domain wall with the clamping pressure, Eq. (23), averaged over the domain wall length, L. This results in the following estimate for the coercive field

$$E_c(t) = \frac{2}{P_s L} \int_0^{L/2} dz P_{cl}(z,t) \tag{24}$$

where integration over the half-length of the wall accounts for the other end of the domain. Evaluation of the time-dependent coercive field assuming the typical length of the domain

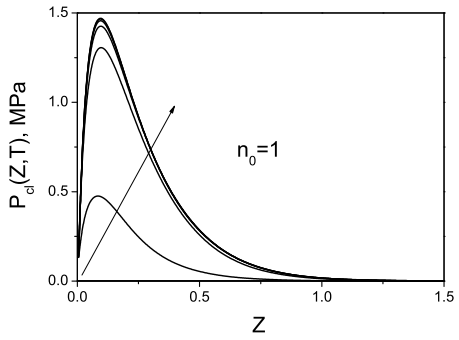

FIG. 10: Snap-shots of the clamping pressure distribution along the domain wall for the succession of times $T = 0$, 0.1, 1, 2, 3, 4, 5 (upwards) for $BaTiO_3$ at room temperature for an oxygen vacancy concentration $c_0 = n_0 \cdot c^*$.

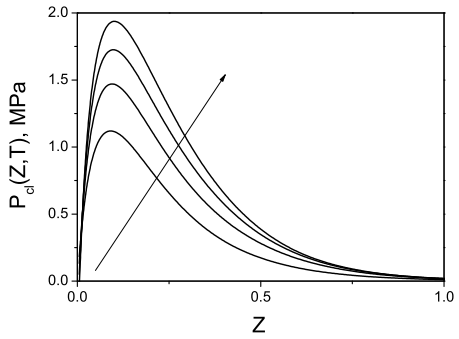

FIG. 11: The saturated clamping pressure distribution along the domain wall for $BaTiO_3$ at room temperature for the oxygen vacancy concentrations $c_0 = n_0 \cdot c^*$ with $n_0 = 0.5$, 1, 1.5 and $n_0 = 2$ (upwards).

wall $L = 20a$ obtains a characteristic value of $E_c \simeq 1$ kV/cm which is of the order of the coercive field in unaged bulk samples of $BaTiO_3$ [7, 8]. In fact, the magnitude of the clamping pressure and, consequently, the value of the coercive field may be substantially larger then it was estimated using Eq. (24). Firstly, the peak value of the pressure has to be approximately doubled if one takes into account the reduction of the energy of electrostatic field in the dielectric material outside the grain which is approximately the same as in the ferroelectric area assuming $\varepsilon_d = \varepsilon_f$. Secondly, the consideration of the anisotropy of the

dielectric constant is expected to scale up the pressure together with the energy gain by the factor of $\sqrt{\varepsilon_a/\varepsilon_c}$ which is about 6 for $BaTiO_3$. Finally, values of few MPa are expected for the average clamping pressure at the domain wall and the values of few kV/mm are expected for the coercive field due to charge carrier migration which is in agreement with the characteristic values observed on the aged samples of $BaTiO_3$ [7, 8]. Accordingly, the coercive field, Eq. (24), multiplied by the factor of 12 is shown in Fig. 12 in physical units to compare with known experimental data. The dashed line shows that the time behavior of E_c mimics logarithmic time dependence for durations less then a few τ_μ.

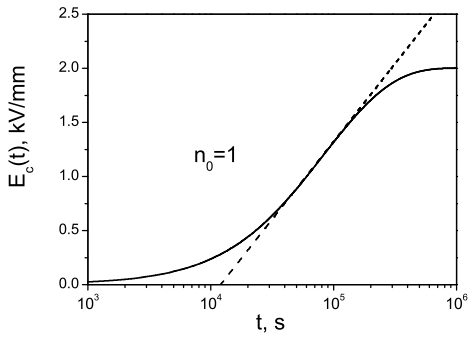

FIG. 12: Coercive field due to charged defect migration as a function of time (solid line) for the oxygen vacancy concentration $c_0 = n_0 \cdot c^*$. Dashed line shows fitting with logarithmic dependence for intermediate times.

One more essential factor which brings about enhancement of the coercive field is that the minimum energy of the system will further substantially decrease if domain wall bending is allowed contributing to the increase of the clamping pressure, Eq. (23). This mechanism is, however, beyond the consideration in our model of rigid walls.

The above obtained values are much larger than typical magnitudes of clamping pressure arising due to dipole re-orientation [14]. Indeed, for uniformly aligned dipoles in the latter mechanism, the dipole moments exert upon the domain wall a clamping pressure $P_{or} \simeq c_0 E_z d$ where the dipole moment $d = q_f l/2$ with the dipole length of $l = 4 \cdot 10^{-10}$m. For the material parameters assumed in the above estimations and $c_0 = c^*$ this results in the peak value of the clamping pressure $P_{or} = 9.7\,\mathrm{kPa}$ which is two orders of magnitude smaller than that in the drift mechanism.

A common feature of these two aging mechanisms is that both dipole re-orientation and defect migration occur in those areas where a depolarization electric field is present. In respect thereof these mechanisms can be classified neither as volume nor as boundary ones as was suggested in the recent works by Zhang and Ren [7, 8] but rather as geometry dependent. Indeed, in the two-dimensional periodic array of domains considered here the depolarization field is present only near the grain boundaries causing both defect drift and dipole re-orientation only in this area. On the other hand, in the single domain state of a Mn-doped $BaTiO_3$ single crystal observed in Ref. [8] a one-dimensional geometry is virtually realized where the depolarization field is present in the whole sample [29] and invokes both dipole re-orientation and defect drift in the whole volume.

V. CONCLUSIONS

In this work, we have considered migration of charged defects as a possible reason for aging in ferroelectrics. The model is based on two main assumptions: 1) existence of mobile carriers of ionic or electronic nature in the bulk material and 2) presence of strong local depolarization fields due to bound charges at the domain faces. The first assumption is based on direct measurements of the conductivity in perovskites [26], the second one was at least partly confirmed in observations of Ref. [6]. Solving self-consistently the drift-diffusion equation together with the Gauss equation for the fixed two-dimensional domain array [34, 35, 36, 37] reveals gradual formation of space charge zones compensating the field generated by charged domain faces. Charged domain walls, which are tip-to-tip or tail-to-tail configurations of the polarization in adjacent domains, are electrically equivalent to our model. The biggest difference arises due to the fact that charged domain walls are often observed as needle tip domains in single crystals [45]. The geometry is thus considerably different from the model of parallel domain walls presented in our paper, where only periodic straight domain configurations are captured.

The process of charge defect migration is accompanied by the reduction of the energy of the electrostatic depolarization field which leads to the energy minimum where the system will resist any change of the domain pattern. The characteristic time of this relaxation depends on the doping and is typically about $5 \cdot \tau_\mu \simeq 8 \cdot 10^5$ s $\simeq 9$ days, where τ_μ is a time of drift over the distance of domain width. That is why, after aging, a clamping force at

a domain wall arises if an external electric field attempts to shift the domain wall from its initial position. This force may be estimated from the calculated energy gain due to the reduction of the depolarization field. The peak value of the clamping pressure is in the range of $1 \div 10\,\mathrm{MPa}$ but the pressure is distributed very inhomogeneously along the domain wall concentrating near the domain ends. Nevertheless, the total value of the clamping force at the domain wall results in the characteristic coercive field of few kV/mm which is comparable with that observed on the aged samples of Mn-doped $BaTiO_3$ [8].

Clamping pressures on domain walls in the presented two-dimensional model are considerably lower than in the uniaxial case [29] and approach macroscopically observable values. They are two orders of magnitude larger than in the picture of defect dipole re-orientation [14] and are thus a plausible mechanism for aging in ferroelectrics. In contrast to the one-dimensional case with only one characteristic value of electric field, $E_d = P_s/\varepsilon_f\varepsilon_0$, treated earlier [29] the two-dimensional model exhibits seemingly a wide spectrum of characteristic times according to the position-dependent values of the electric field $\mathbf{E}(x, y)$. This allows one to expect a time dependence of the clamping pressure in a two-dimensional array of domains different from the one-dimensional case [29]. Nevertheless, comparing time evolution of the field and defect concentration in Ref. [29] with Figs. (4,5,6,7) one observes a striking similarity between them. We are thus concerned with a single characteristic time constant $\tau_r = \tau_\mu/n_0$ characterizing the relaxation of the system. This time is independent of the width of the domains, a. In fact, $\tau_r = \varepsilon_f\varepsilon_0/\lambda$ with $\lambda = q_f c_0 \mu$ being the conductivity of the material is the Maxwell relaxation time which only depends on the mobility and local concentration of the mobile carriers. This in turn means that a distribution of grain sizes in the material and accordingly a distribution of domain sizes does not entail a distribution of characteristic relaxation times. The logarithmic time dependence of the dielectric constant during aging yet remains to be explained.

A crucial parameter for the plausibility of the time scale in our simulations is the mobility of charged species in a ferroelectric material. The mobility of oxygen vacancies considered is still a highly disputable issue. The activation barrier for this ionic defect is usually estimated in the range of 0.9-1.1 eV in both experimental works and first principle calculations [46, 47, 48, 49] which makes the migration of oxygen vacancies over the distance of the order of the domain width $\simeq 0.5\,\mu$m most unlikely. On the other hand, the estimations of the mobility in the Refs. [26, 30, 50, 51] are similar to or higher than that given in Refs. [40, 41] which

we used for simulations in our study. We would like to stress here therefore that the nature of the charge carriers plays no important role for the model presented. These may be also electronic carriers as was suggested in Refs. [47, 52]. In any case our input parameters agree with direct measurements of the conductivity of perovskites indifferent to the nature of the charge carriers [26].

It is evident that any real system will contain more than one mobile charge carrier. In case their mobilities or concentrations are considerably different, the final distribution of defects of the more mobile / more frequent carrier will determine the field environment for the drift of the second carrier as it was discussed in Ref. [47]. The solutions from the present calculation would have to be taken as starting condition and iteratively the final solution could be found. In case of equal mobilities and concentrations, a coupled system of equations has to be solved which is the issue of forthcoming work. Similarly the local potential wells for the domain wall which determine the dielectric constant will be given in a future publication.

VI. ACKNOWLEDGEMENT

Discussions with Karsten Albe, Nina Balke, Dietmar Gross, Valeriy Ishchuk, Hans Kungl, Ralf Müller, Hermann Rauh, and Jürgen Rödel and the support by the Sonderforschungsbereich 595 of the Deutsche Forschungsgemeinschaft are gratefully acknowledged.

---

[1] M. E. Drougard and D. R. Young, Phys. Rev. **94**, 1561 (1954).

[2] M. C. McQuarrie and W. R. Buessem, Ceram. Bull. **34**, 402 (1955).

[3] M. Takahashi, Jpn. J. Appl. Phys. **9**, 1236 (1970).

[4] H. Thomann, Ferroelectrics **4**, 141 (1972).

[5] K. Carl and K. H. Härdtl, Ferroelectrics **17**, 473 (1978).

[6] G. Arlt and H. Neumann, Ferroelectrics **87**, 109 (1988).

[7] L.X. Zhang and X. Ren, Phys. Rev. B **71**, 174108 (2005).

[8] L.X. Zhang and X. Ren, Phys. Rev. B **73**, 094121 (2006).

[9] K. W. Plessner, Proc. Phys. Soc. B **69**, 1261 (1956).

[10] S. Ikegami and I. Ueda, J. Phys. Soc. Jpn. **22**, 725 (1967).

[11] P. V. Lambeck and G. H. Jonker, J. Phys. Chem. Solids **47**, 453 (1986).

[12] H.-J. Hagemann, J. Phys. C: Solid State Phys. **11**, 3333 (1978).

[13] J. F. Scott, B. Pouligny, K. Dimmler, M. Parris, D. Butler, and S. Eaton, J. Appl. Phys. **62**, 4510 (1987).

[14] U. Robels and G. Arlt, J. Appl. Phys. **73**, 3454 (1993).

[15] A.G. Chynoweth, Phys. Rev. **117**, 1235 (1960).

[16] V.Ya. Shur, A.L. Gruverman, N.V. Korovina, M.Z. Orlova, and L.V. Sherstobitova, Sov. Phys. Solid State **30**, 172 (1988).

[17] V. Gopalan and M.C. Gupta, Appl. Phys. Lett. **68**, 888 (1996).

[18] M. Imlau, T. Bieringer, S.G. Odulov, and T. Woike, in Nanoelectronics and Information Technology, R. Waser, Ed., Wiley-VCH, Weinheim, 2003.

[19] C. Alemany, B. Jiménez, J. Mendiola, and E. Maurer, J. Mater. Sci. **19**, 2555 (1984).

[20] N. Korneev, H. Veenhuis, K. Buse, and E. Krätzig, J. Optic. Soc. Am. B - Opt. Phys. **18**, 1570 (2001).

[21] S.G. Gakh, E.D. Rogach, and E.V. Sviridov, Techn. Phys. (Russ.) **46**, 47 (2001).

[22] V. Mueller, Y. Shchur, H. Beige, S. Mattauch, J. Glinnemann, and G. Heger, Phys. Rev. B **65**, 134102 (2002).

[23] V. Mueller, H. Beige, and Y. Shchur, Ferroelectrics **290**, 151 (2003).

[24] V. Mueller and Y. Shchur, Europhys. Lett. **65**, 137 (2004).

[25] P. Paruch, T. Giamarchi, and J.M. Triscone, Phys. Rev. Lett. **94**, 197601 (2005).

[26] R.M. Waser, J. Am. Ceram. Soc. **74**, 1934 (1991).

[27] G. Arlt and U. Robels, Integrated Ferroelectrics **3**, 343 (1993).

[28] R. Lohkämper, H. Neumann, and G. Arlt, J. Appl. Phys. **68**, 4220 (1990).

[29] D.C. Lupascu, Y.A. Genenko, and N. Balke, J. Am. Ceram. Soc. **89**, 224 (2006).

[30] M. Dawber, K.M. Rabe, and J.F. Scott, Rev. Mod. Phys. **77**, 1083 (2005).

[31] R. Williams, J. Phys. Chem. Solids **65**, 399 (1965).

[32] V. Ravikumar, R.P. Rodrigues, and V.P. Dravid, J. Am. Ceram. Soc. **80**, 1117 and 1131 (1997).

[33] G.E. Pike, W.L. Warren, D. Dimos, B.A. Tuttle, R. Ramesh, J. Lee, V.G. Keramides, and J.T. Evans, Jr., Appl. Phys. Lett. **66**, 484 (1995).

[34] C. Kittel, Phys. Rev. **70**, 965 (1946)

[35] L.D. Landau and E.M. Lifshitz, *Theoretical Physics, Vol. VIII: Electrodynamics of Continuous Media* (Pergamon, Oxford, 1963).

[36] T. Mitsui and J. Furuichi, Phys. Rev. **90**, 193 (1953)

[37] V.N. Fedosov and A.S. Sidorkin, Sov. Phys. Solid State **18**, 964 (1976)

[38] A.P. Prudnikov, Y.A. Brychkov, and O.I. Marychev, *Integrals and Series* (Gordon and Breach, New York, 1986).

[39] J.D. Jackson, *Classical Electrodynamics* (John Wiley & Sons, New York, 1975).

[40] R. Wernicke, Dissertation RWTH-Aachen, Germany (1975).

[41] B. Jaffe, W.R. Cook, Jr., and H. Jaffe, *Piezoelectric Ceramics* (Academic Press, Marietta, OH, 1971).

[42] U. Hennings, *private communication* (2005).

[43] V.N. Nechaev and A.M. Roschupkin, Ferroelectrics **90**, 29 (1989).

[44] E.K.H. Salje and Y. Ishibashi, J. Phys.: Condens. Matter **8**, 8477 (1996).

[45] V.Ya. Shur, E.L. Rumyantsev, E.V. Nicolaeva, and E.I. Shishkin, Appl. Phys. Lett. **77**, 3636 (2000).

[46] A.K. Tagantsev, I. Stolichnov, E.L. Colla, and N. Setter, J. Appl. Phys. **90**, 1387 (2001)

[47] R. Meyer, R. Lidtke, and R. Waser, Appl. Phys. Lett. **86**, 112904 (2005)

[48] D. Damjanovic, *Hysteresis in Piezoelectric and Ferroelectric Materials*, in *The Science of Hysteresis*, ed. by I. Mayergoyz and G. Bertotti (Elsevier, 2005)

[49] P. Erhart and K. Albe, to be published

[50] M. Dawber and J.F. Scott, Appl. Phys. Lett. **76**, 1060 (2000)

[51] A.Q. Jiang, J.F. Scott, and M. Dawber, J. Appl. Phys. **92**, 6756 (2002)

[52] W.L. Warren, D. Dimos, B.A. Tuttle, G.E. Pike, R.W. Schwartz, P.J. Clews, and D.C. McIntyre, J. Appl. Phys. **77**, 6695 (1995)